Supplementary Information

Multi-Stable Soft Robots Assembled from Bistable Auxetic Building Blocks

*Bojian Zhang, Zhiqiang Meng, Xudong Yang, Yiran Zhang, Tianyu Chen, Yu Chen, and Yifan Wang**

This PDF file includes:

Supplementary documents:

S1. Materials and methods

S2. Theoretical model

S3. Manipulator geometry parameters in bending experiment

S4. Details of MATLAB control algorithm

Figure. S1 to S8

Video S1 to S8

Table S1 to S2

S1. Materials and methods

S1.1 Characterization of materials

To determine the stress-strain curves of TPU at room temperature (room temperature), uniaxial tensile tests were conducted on dog-bone-shaped specimens (Figure S1A). The material testing machine is (Mark-10 Corp) equipped with a 100 N load cell. The specimens shown in Figure S1A were fully clamped at both ends and stretched at a strain rate of 0.2 min^{-1} at room temperature.

The stress-strain curves measured (Figure S1B), indicate that TPU can be accurately modeled using the Mooney-Rivlin hyperelastic model. The corresponding material parameters can be identified as follows: for TPU, $C_{10} = -10.85$ MPa and $C_{01} = 23.98$ MPa, with Young's modulus given by $E = 6\left(C_{01} + C_{10}\right) = 78.4$

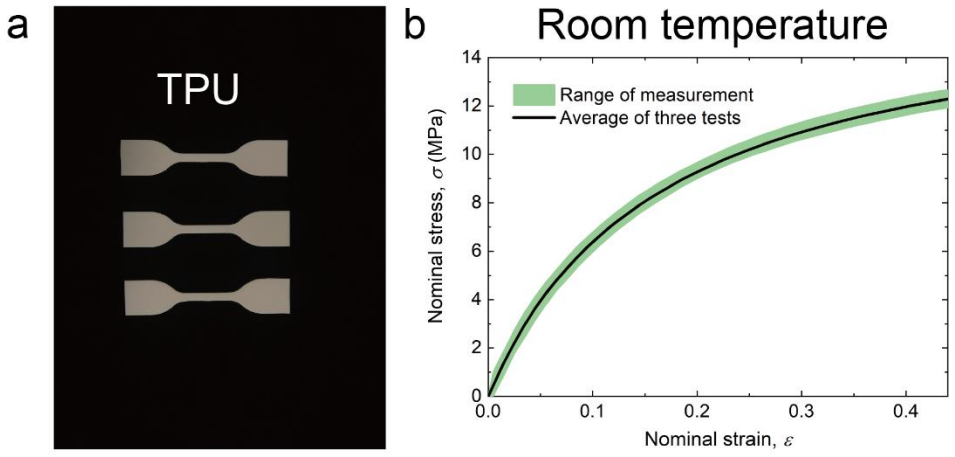


Figure S1. Measured uniaxial nominal stress-strain curves of TPU at room temperature. a) Dog-bone shaped plate specimens. b) The corresponding stress-stain curves

S2. Theoretical model

S2.1 Mechanical model of bistable auxetic building blocks

In the main text, we simplify one part of auxetic building block into a mechanical model which included three beams as rigid bar and two hinges as combination of torsion and compression spring. Due to the boundary conditions of each beam, we have three assumptions to simplify the model: 1. For compression spring, it always collineation with beam CD; 2. For torsion spring, rotation angle θ is equal $\pi - \theta_{\mathrm{ABC}}$; 3. We consider hinge BC and DE are same in compression and torsion. Hence, due to the boundary condition, we can obtain the relationship between rotation angle θ and beam displacement u as:

$$\theta = \arctan \frac{u}{L + 2l - u} \tag{S1}$$

Also, we have the relationship between compression distance and beam displacement u as:

$$\Delta = 2l + L - \sqrt{(L + 2l - u)^2 + u^2} \tag{S2}$$

Regarding to Hooke's law, we have energy equation for compression springs K_l:

$$\Delta_{\mathrm{BC}} = \Delta_{\mathrm{DE}} = \frac{1}{2}\Delta \tag{S3}$$

$$\begin{aligned} W_{\mathrm{l}} &= \frac{1}{2} K_{\mathrm{l}} {\Delta_{\mathrm{BC}}}^2 + \frac{1}{2} K_{\mathrm{l}} {\Delta_{\mathrm{DE}}}^2 \\ &= \frac{1}{4} K_{\mathrm{l}} \Delta^2 = \frac{1}{4} K_{\mathrm{l}} \left(2l + L - \sqrt{(L + 2l - u)^2 + u^2} \right)^2 \end{aligned} \tag{S4}$$

And energy equation for torsion springs K_t:

$$W_{\mathrm{tBC}} = \frac{1}{2} K_{\mathrm{tBC}} \theta^2 = W_{\mathrm{tDE}}$$
$$W_{\mathrm{t}} = 2 \times \frac{1}{2} K_{\mathrm{tBC}} \left(\arctan \frac{u}{L + 2l - u} \right)^2 \tag{S5}$$

And total energy in half piece:

$$W = W_{\mathrm{t}} + W_{\mathrm{l}} \tag{S6}$$

$$W = W\left(u \middle| K_{\mathrm{t}}, K_{\mathrm{l}}, l, L\right) \tag{S7}$$

2.2 Determination of stiffness K_{t} and K_{l}

With the help pf FEA simulation, we calculate the stiffness of the torsion spring K_{t} and compression spring K_{l} in terms of the geometrical parameters b, t, l and the material parameters E.

Here, we consider compression spring stiffness K_{l} first. Through dimensional analysis, K_{l} can be assumed as form of

$$K_{\mathrm{l}} = \lambda_2 \frac{Ebt}{l} \tag{S8}$$

Where λ_2 is a dimensionless coefficient. Through FEA simulation of interconnected ligaments with different size, it can be obtained as

$$\lambda_2 = -1.1\frac{t}{l} + 1.2 \tag{S9}$$

Then, we consider torsion spring stiffness K_t. Similarly, through dimensional analysis, K_t can be assumed as:

$$K_t = \lambda_1 \frac{Ebt^3}{l} \tag{S10}$$

Where λ_1 is a dimensionless coefficient. Through FEA simulation of interconnected ligaments with different size, it can be obtained as

$$\lambda_1 = 2.3609 \times \exp\left(-27.692 \frac{t}{l}\right) + 0.11196 \tag{S11}$$

To evaluate K_t and K_l, we calculated the force-displacement curves of the part with shifty geometrical parameters using FEA. Figure. S2B presents the force-displacement curves of TPU hinges with different thickness in compression simulation. Figure. S2E presents the moment-rotation angle curves if TPU hinges with different thickness in torsion simulation. By fitting the FEA results with Equation S8 and S10, the value of λ_1 and λ_2 can be determined (Figure S2C and Figure S2F).

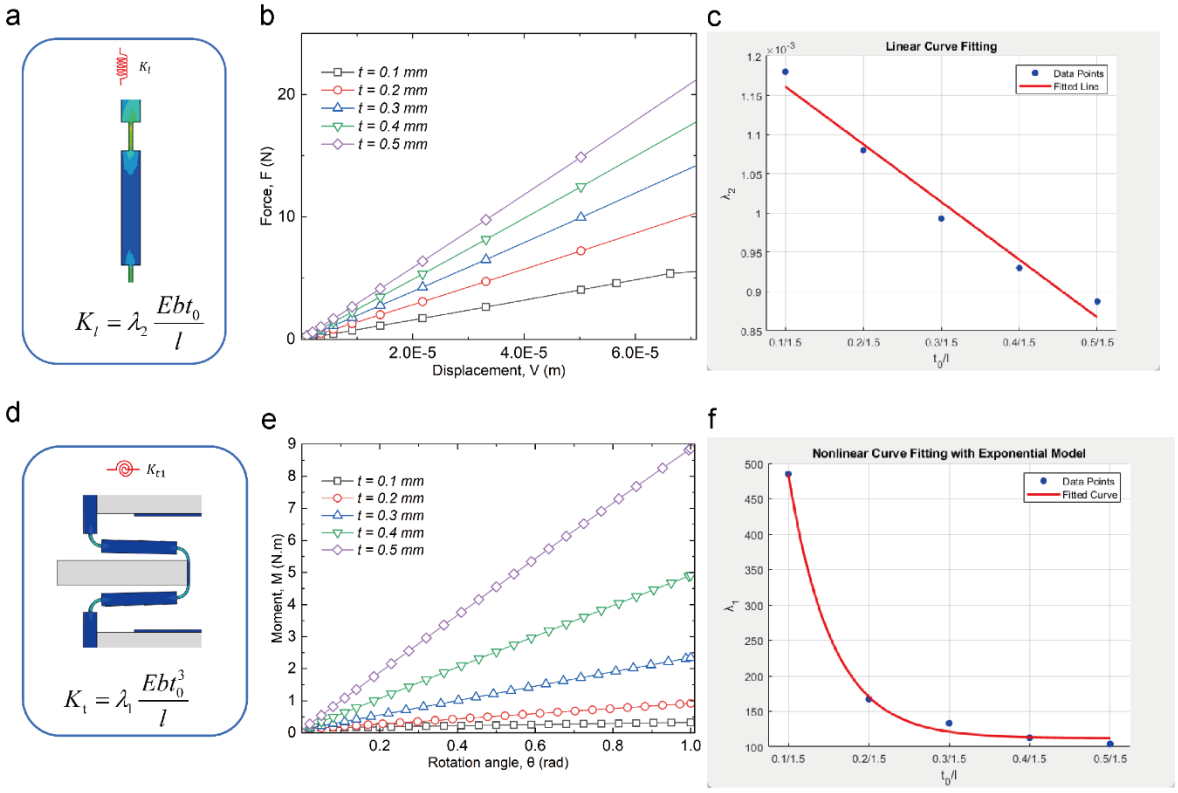


Figure S2. FEA simulation resulting and fitting curves of λ_1 and λ_2. a) FEA snapshot of specimen in compression spring stiffness simulation. b) Force-displacement curves with different parameters in compression simulation. c) Linear fitting curve for coefficient λ_1. d) FEA snapshot of specimen in torsion spring stiffness simulation. e) Force-displacement curves with different parameters in bending simulation. f) Nonlinear fitting curve for coefficient λ_2.

Then, we have all parameters of energy equation W. Combining all the parameter into energy equation, we have:

$$W_t = 2 \times \frac{1}{2} K_{tBC} \left(\arctan \frac{u}{L + 2l - u} \right)^2 \tag{S12}$$

$$W_l = \frac{1}{4} K_l \Delta_{BE}^2 = \frac{1}{4} K_l \left(2l + L - \sqrt{(L + 2l - u)^2 + u^2} \right)^2 \tag{S13}$$

$$
\begin{aligned}
W &= W_{\mathrm{t}} + W_{\mathrm{l}} \\
&= 2 \times \frac{1}{2} K_{\mathrm{tBC}} \left(\arctan \frac{u}{L + 2l - u} \right)^2 + \frac{1}{4} K_{\mathrm{l}} \left(2l + L - \sqrt{(L + 2l - u)^2 + u^2} \right)^2
\end{aligned} \tag{S14}
$$

Then we rewrite Equation S14 by divided $Ebtl$ on both sides:

$$
W^* = \frac{W}{Ebtl} \tag{S15}
$$

From the equation $W^* = W^*\left(u/l \middle| t/l, l/L\right)$, we can obtain that for bistable case, the curvature is increasing at first and then decreasing; however, for monostable case, the curvature monotone increasing. Hence, we can define:

$$
\eta = \frac{W_{\max} - W_{\min}}{W_{\max}}
$$

for bistable cases, $\eta > 0$; for monostable cases $\eta = 0$. Then, the phase diagram of $\eta = \eta\left(t/l, l/L\right)$ is obtained in Figure 2B. We picked some random value of t/l and l/L in FEM and experiment to verify the mechanism theory is correct, and results matching well.

S3. Manipulator geometry parameters in bending experiment

Firstly, each of the five building blocks within one pneumatic muscle is distinctively designed. We varied their hinge lengths, for instance: we started from $t = 0.1$ mm and $l = 1.5$ mm, then subsequently increased l by 0.25 mm until reaching $l = 2.5$ mm. Therefore, we have five blocks with varying energy barriers (Figure 2D). When increasing negative pressure in the pneumatic muscle, we can fold the five blocks in sequence. Video S6 demonstrates the relationship between negative pressure and the number of folded blocks. As observed, with increasing negative pressure, the number of folded blocks tends to linearly increase. At -8 kPa, all five building blocks are in a folded state. Regarding the query about changing bending amplitude, it linearly varies from 10.0 mm to 69.8 mm as the number of folding blocks increases from 1 to 5. Table S1 presents the relationship between the number of folding blocks, bending angle, and bending amplitude.

Table S1. Manipulator bending geometry parameters with folding block number.

Air pressure (kPa)	Folding block number	Contracted muscle length (mm)	Bending angle (°)	Bending radius (mm)
0	0	21.5	0	∞
-2	1	19.5	16	69.8
-3	2	18.5	32	33.1
-4	3	17	48	20.3
-5	4	16	64	14.3
-8	5	14	80	10.0

S4. Details of MATLAB control algorithm

The detail of control algorithm in MATLAB software is presented in Figure S5. Here, we insert a pseudocode to demonstrate how the algorithm deals with captured data and make decisions for STM32 board:

Control algorithm goes through the following steps:

1. Initialize:

$u_{\text{cmd}} = \left[u^x, u^y \right]$ // Human operator's command

$S_i = \left[s_i^1, s_i^2, s_i^3 \right]$ S for i in range (1, 217) // All possible 3D positions

$u_{\text{in}} = \left[u^x, u^y \right]$ for i in range (1, 217) // Corresponding command inputs

$Loop_{flag} = True$ // Flag to continue loop

2. Ground Truth Collection:

Collect and label $\left\{ S_i, u_{\text{in}} \right\}$ meticulously prior to experiment

3. Main Control Loop:

While $Loop_{flag}$:

3.1 Operator Intent Estimation:

$i^* = \arg\min \left\| u_{\text{in}} - u_{\text{cmd}} \right\|_2$ // Estimate operator's intent

$S_i = \left[s_i^1, s_i^2, s_i^3 \right]$ // Corresponding state

3.2 Current State Inference:

p = captured raw sensor input

$S_c = f(p)$ // Inference from vision-based sensory system

3.3 Relay Control Determination:

$u_{\text{out}} = sign\left(sat\left(S_{i^*} - S_c\right)\right)$ // Determine relays' controls

// sat denotes the saturation function

3.4 Check for Transition to Locked State:

If $\left|S_{i^*} - S_c\right|$ is small:

Transition system into a locked state

$Loop_{flag} = False$ // Exit the loop

3.5 Update System State:

// Update the system state based on control output u_{out}

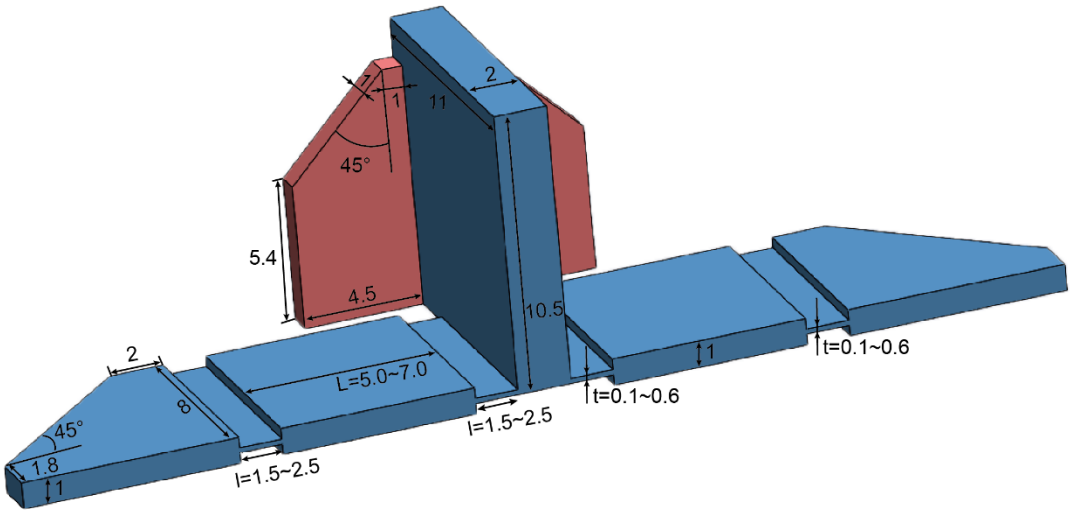


Figure S3. Design and dimensions of the single part in cross section-view.

Table S2. The meaning of important dimensions in bistable auxetic block design.

Parameter	Implication	Value in Exp	Unit
l	Length of hinges	1.5~2.5	mm
t	Thickness of hinges	0.1~0.5	mm
L	Length of beams	5.0~7.0	mm
u	Displacement of beams	0~16	mm
θ	Rotation angle of beams	0~90	°
Δ	Deformation of beams	\	\
K_t	Coefficient value of the torsion spring	\	\
K_l	Coefficient value of the compression spring	\	\
λ_1	Fitting parameter of the torsion spring	\	\
λ_2	Fitting parameter of the compression spring	\	\

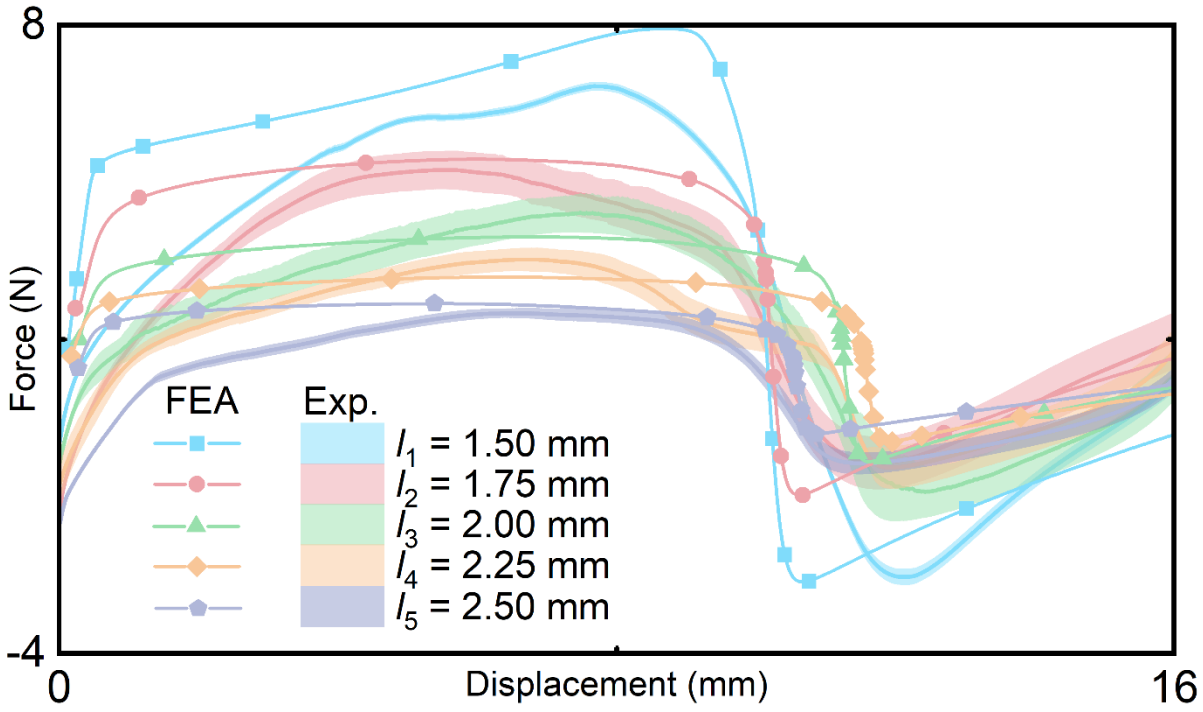


Figure S4. Individual force-displacement curves in FEA and experiment for the five blocks within the multi-stable structure.

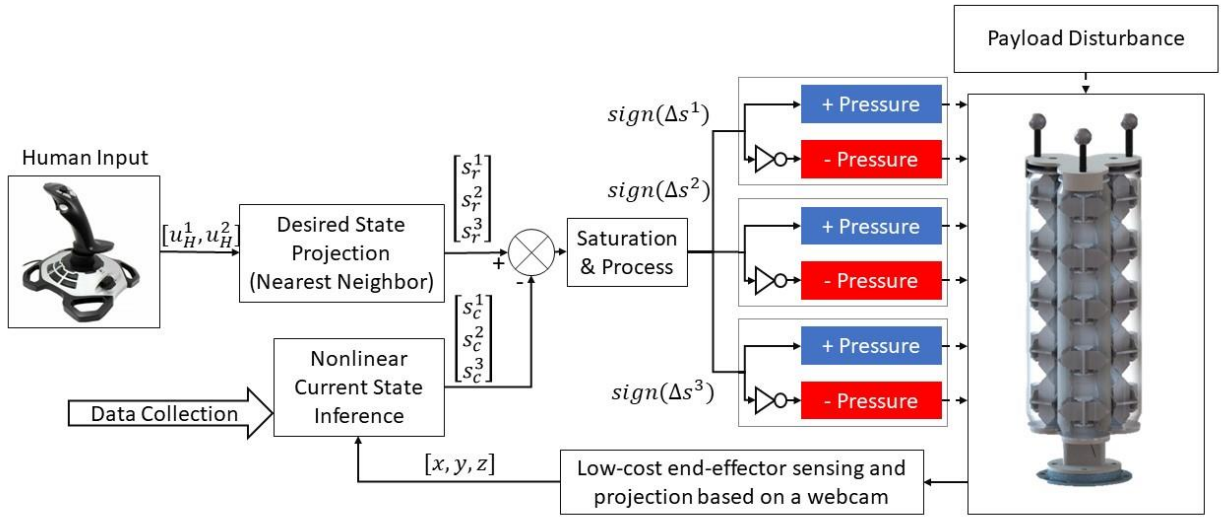


Figure S5. Close-loop control diagram of multi-stable manipulator.

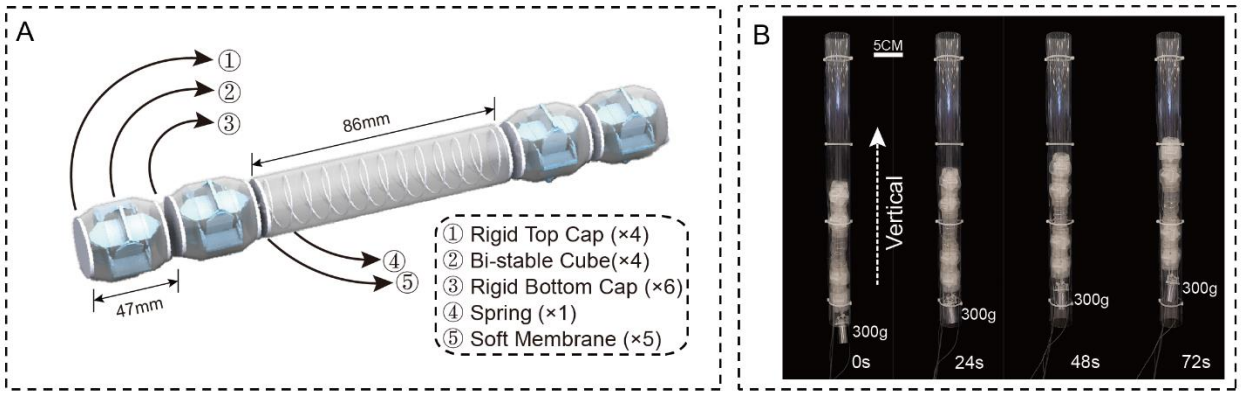


Figure S6. Bistable tube crawler with multi anchors. a**)** Design and dimensions of multi-anchors bistable tube crawler. b) Snapshots of the crawler locomotion with zero loading and 300 g loading in vertical direction (1.25 mm/s).

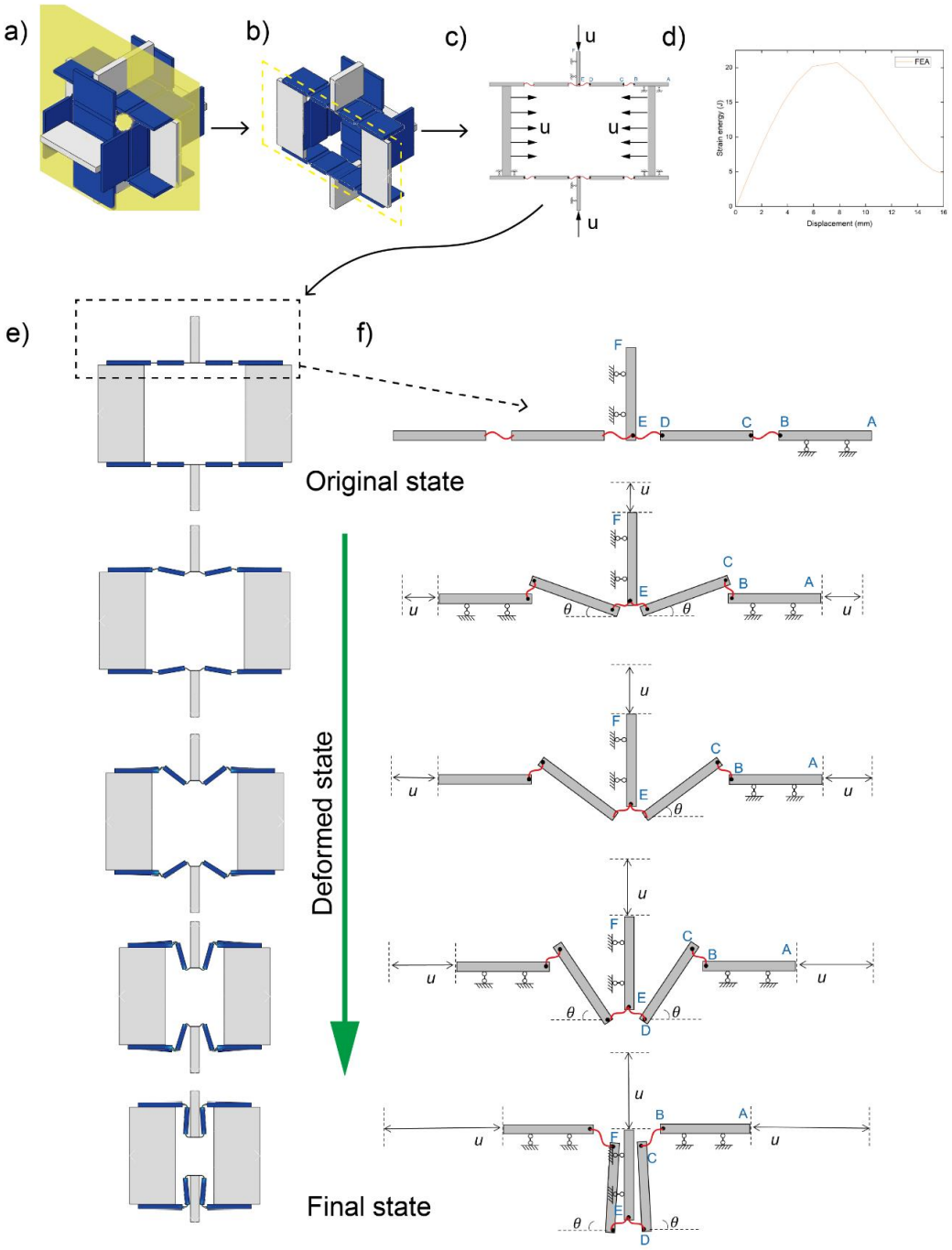


Figure S7. Schematic of a bitsable auxetic block and its deformation upon loading. a) Bistable auxetic block model in FEA. b) Cutaway view of block. c) Deformation response of the block to vertical compression. d) Strain energy and displacement curve of bistable auxetic block in FEA. e) Sequential deformations of the block and f) their corresponding simplified mechanical models using only a twelfth of the block.

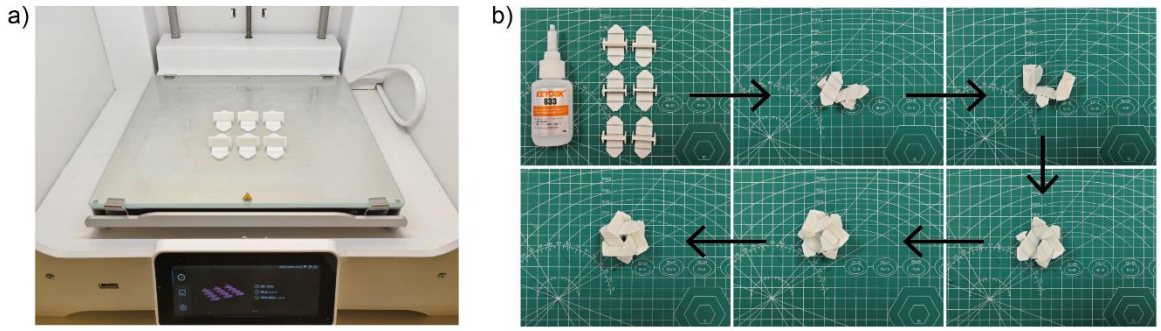


Figure S8 Fabrication of bistable auxetic blocks by FDM. a) 3D printing process for manufacturing a single part of the bistable auxetic block using TPU filament. b) Assembling process of the bistable auxetic block by gluing the printed parts together.

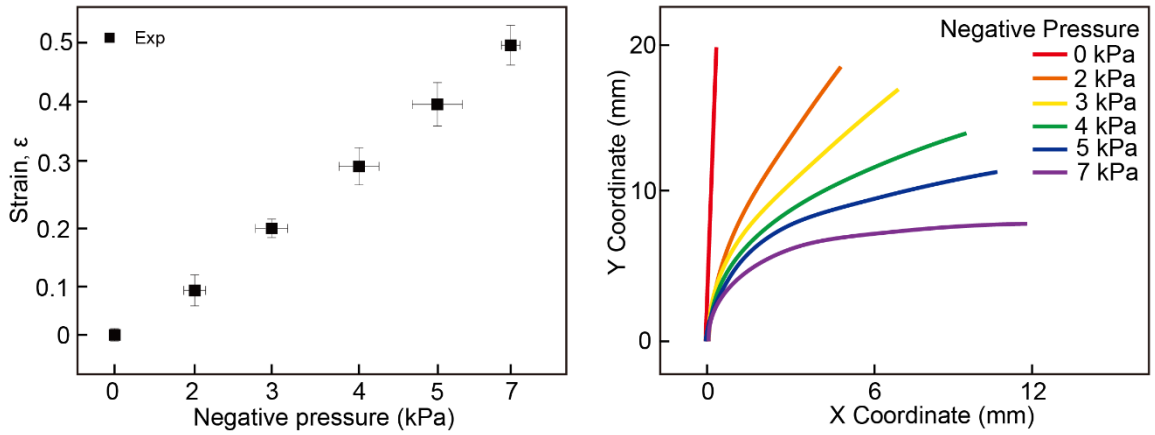


Figure S9 a) Relationshio between the contraction/expansion ratio and applied pressure. b) relationship between bending curvature and applied pressure.

Video S1.

Experiment of loading capacity.

Video S2.

Multi-stable manipulator with handle input control.

Video S3.

Multi-stable manipulator with hand tracking input control.

Video S4.

Tube crawling robot elongation unit designed with bistable auxetic blocks.

Video S5.

Tube crawling robot elongation unit designed with spring.

Video S6.

Tube crawling robot locomotion with cargo delivery.

Video S7.

Tube crawling robot crawled in soft tube (LDPE).

Video S8.

Experimental pressure control for the multi-stable pneumatic muscle.